were detached from the plate with trypsin. They were centrifuged at 500×g for 5 min, and the cell pellet was suspended in 0.2 ml of PBS. The suspension was stored at −80°C until use. The samples were allowed to thaw and were refrozen once more at −80°C before being thawed for use in the assay (two rounds freeze/thaw). Glutathione activity of the cell lysate was measured colorimetrically using the Bioxytech GSH-420 (OXIS International, Portland, OR, USA). Protein concentrations in lysates were determined by the method described for the amino acid transport measurement.

Data (mean ± standard deviation) were analyzed and compared with one-way analysis of variance with post-hoc Turkey-Kramer. A p-value <0.05 was considered statistically significant.

Results

Effects of glutamine concentration on cell growth

As shown in Fig. 1, cell growth rates were dependent on glutamine concentrations. Cell number significantly decreased in the glutamine-deprived groups compared with control, and significant differences were found among the four groups ($p<0.01$).

Effects of glutamine deprivation on glutamine and glutamate transport

The transport of glutamine and glutamate was linear for at least 3 min, and Na^+-dependent glutamine and Na^+-dependent glutamate uptake represented 95% and 70% of total uptake, respectively. Therefore, 1-min assays of glutamine and glutamate transport were chosen for subsequent experiments. As shown in Fig. 2, Na^+-dependent glutamine transport significantly decreased in 200-μM (2418 ± 267 pmol/mg protein/min) and 0-μM (1909 ± 92 pmol/mg protein/min) glutamine compared with control (3480 ± 226 pmol/mg protein/min) and 400 μM (3366 ± 84 pmol/mg protein/min) glutamine ($p<0.01$). There was a significant decrease in 0-μM glutamine compared with 200-μM glutamine ($p<0.05$).

Fig. 3 shows the effects of glutamine deprivation on total, Na^+-dependent, and Na^+-independent glutamate transport. Total and Na^+-independent glutamate

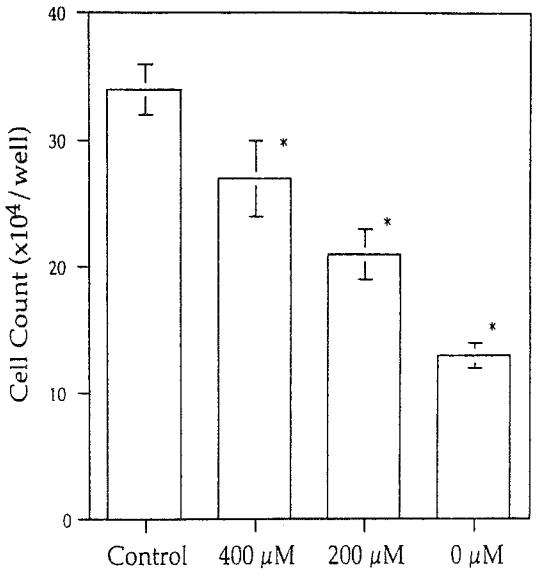

Fig. 1 Effects of glutamine deprivation on cell growth after 2 days. Data are presented as mean ± standard deviation of triplicate determinations. Control represents 2 mM glutamine. *$p<0.01$ vs. other three groups

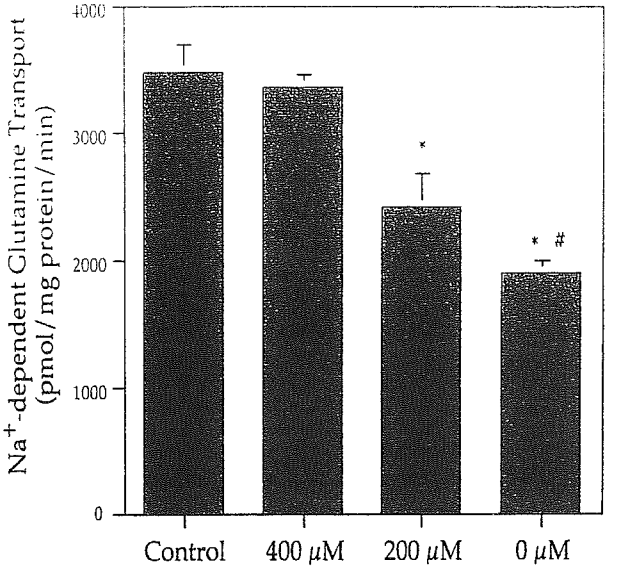

Fig. 2 Effects of glutamine deprivation on Na^+-dependent glutamine transport after 24 h. Data are means ± standard deviation of quadruplicate determinations. *$p<0.01$ vs. control (2 mM glutamine), 400 μM glutamine, #$p<0.05$ vs. 200 μM glutamine

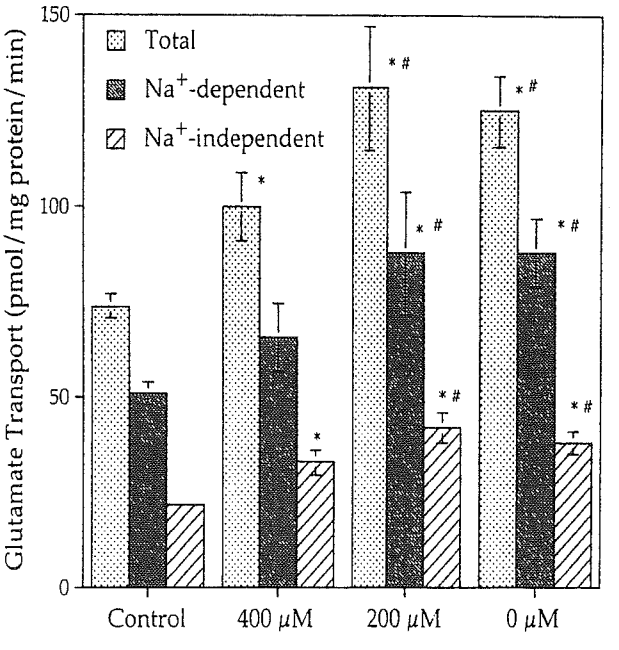

Fig. 3 Effects of glutamine deprivation on total, Na^+-dependent, and Na^+-independent glutamate transport after 24 h. Data are means ± standard deviation of quadruplicate determinations. *$p<0.01$ vs. control (2 mM glutamine), #$p<0.05$ vs. 400 μM glutamine

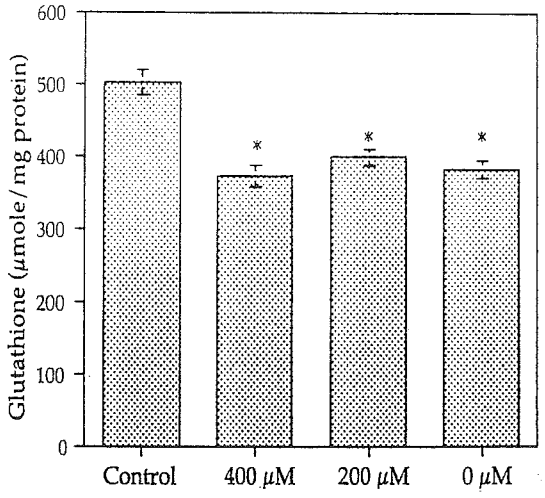

Fig. 4 Effects of glutamine deprivation on glutathione levels after 24 h. Data are presented as mean ± standard deviation of triplicate determinations. *$p < 0.01$ vs. control (2 mM glutamine)

transport significantly increased in 400-μM (total, 100 ± 9; Na^+-independent, 33 ± 3 pmol/mg protein/min), 200-μM (total, 131 ± 16; Na^+-independent, 42 ± 4 pmol/mg protein/min), and 0-μM (total, 125 ± 9; Na^+-independent, 38 ± 3 pmol/mg protein/min) glutamine compared with control (total, 74 ± 3; Na^+-independent, 22 ± 3 pmol/mg protein/min) ($p < 0.01$). Na^+-dependent glutamate transport significantly increased in 200-μM (88 ± 16 pmol/mg protein/min) and 0-μM (88 ± 9 pmol/mg protein/min) glutamine compared with control (51 ± 3 pmol/mg protein/min) ($p < 0.01$). Total, Na^+-dependent, and Na^+-independent glutamate uptake in 200-μM and 0-μM glutamine significantly increased compared with 400-μM glutamine ($p < 0.05$). There were no significant differences between 200-μM and 0-μM glutamine.

Effects of glutamine deprivation on glutathione levels

As shown in Fig. 4, there was a significant decrease in glutathione levels in 400-μM (375 ± 15 μMole/mg protein), 200-μM (400 ± 12 μMole/mg protein), and 0-μM (383 ± 13 μMole/mg protein) glutamine compared with control (503 ± 18 μMole/mg protein, $p < 0.01$), but no significant differences were found among the three glutamine-deprived groups.

Effects of glutamine deprivation on DNA and protein synthesis

Glutamine deprivation resulted in remarkable decreases in ^{3}H-thymidine incorporation, with significant differences among the four groups (control, 39228 ± 3662; 400 μM, 31925 ± 1764; 200 μM, 23256 ± 1666; 0 μM, 13668 ± 970 cpm/mg protein/hr, $p < 0.01$). ^{3}H-leucine incorporation significantly decreased in glutamine-deprived groups (400 μM, 977 ± 66; 200 μM, 814 ± 29; 0 μM, 771 ± 61 cpm/mg protein/hr) compared with control (1104 ± 50 cpm/mg protein/h) ($p < 0.01$), and a significant decrease was found in 200-μM and 0-μM glutamine compared with 400-μM glutamine ($p < 0.01$) (Fig. 5).

Discussion

SK-N-SH neuroblastoma cells responded to glutamine deprivation by increasing total, Na^+-dependent, and Na^+-independent glutamate transport, although glutamine deprivation resulted in the decrease of glutamine transport. The increase in glutamate transport was remarkable in lower glutamine levels. The adaptive increase in amino acid transport elicited by glutamine deprivation has already been reported [12–14]. We have shown the adaptive increase of leucine (system L) and Me-AIB [2-(methylamino) isobutyric acid, a substrate for system A] transport in glutamine-deprived SK-N-SH [15]. Because glutamine is used in several disparate metabolic pathways, SK-N-SH neuroblastoma cells may replace metabolic intermediates normally provided by glutamine with the carbon skeletons and nitrogen of other amino acids when the glutamine availability is limited.

Glutamate is formed by the hydrolysis of glutamine via the enzyme glutaminase and transamination

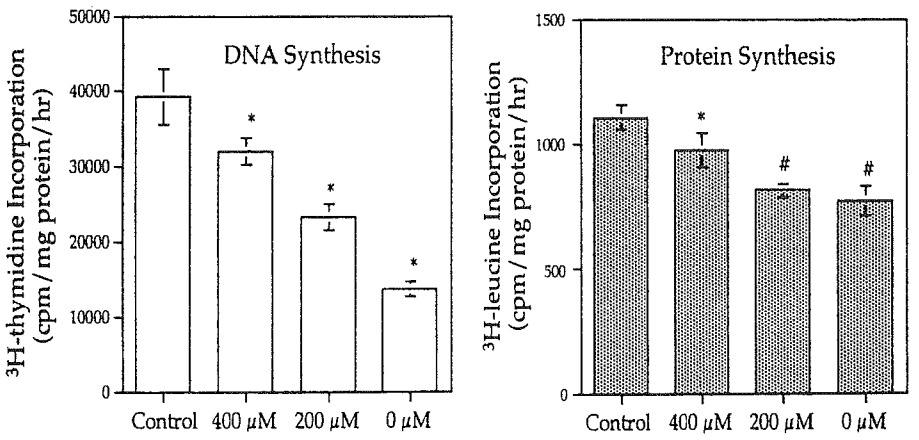

Fig. 5 Effects of glutamine deprivation on ^{3}H-thymidine (DNA synthesis) and ^{3}H-leucine (protein synthesis) incorporation after 24 h. Data are presented as mean ± standard deviation of quadruplicate determinations. *$p < 0.01$ vs. other three groups, #$p < 0.05$ vs. control (2 mM glutamine), 400 μM glutamine

reactions that use glutamine as an amine donor. Therefore, glutamine provides a major source for intracellular production of glutamate, a precursor of glutathione. High intracellular glutathione levels in tumors have been associated with high proliferation rates [16] and drug resistance [17]. For example, intracellular glutathione levels are 2.6–2.8-fold higher in renal cell carcinoma than those in the renal cortex [4]. In the present study, intracellular glutathione levels were maintained in 0-μM glutamine with the same levels found in 400-μM and 200-μM glutamine, although glutamine deprivation resulted in the decrease of its levels by 20% compared with control. Total, Na^+-dependent, and Na^+-independent glutamate transport increased by 69%, 73%, and 73%, respectively, in 0-μM glutamine compared with control. In the condition of the limited availability of extracellular glutamine, the metabolic pathway via glutamine hydrolysis may not be important for the synthesis of glutathione. Our data that glutamine transport decreased in glutamine-deprived conditions support this concept. For the synthesis of glutathione, SK-N-SH neuroblastoma cells may replace its precursor, glutamate, normally provided by glutamine with glutamate transported through the cell membrane when extracellular glutamine levels are diminished.

In the present study, cell growth rates and biosynthesis of DNA and protein correlated directly with glutamine concentration in culture media. ^{3}H-thymidine incorporation decreased by 19%, 41%, and 70% in 400-μM, 200-μM, and 0-μM glutamine, respectively, compared with control. These results are identical with those of our previous study in adult cancer cell lines [3]. Therefore, the response observed in the present study may not be specific to neuroblastoma cells. As shown in Fig. 1, SK-N-SH cells could survive and even grow in glutamine concentrations lower than normal circulating levels (500–600 μM). The centers of solid tumors are generally poorly vascularized, and intercellular amino acid concentrations can be much lower than the normal circulating levels [18]. Our findings obtained from an *in vitro* cell culture model may not be the same as those observed *in vivo*. However, decreased extracellular amino acid levels encountered by tumors *in vivo* may elicit similar adaptive responses in amino acid transport and glutathione synthesis that contribute to the maintenance of cytoplasmic amino acids and glutathione levels.

Collectively, our results, as presented here, support the concept that glutamine mediates neuroblastoma cell proliferation by regulating glutathione synthesis and amino acid transport across the cell membrane, both when sufficient nutrients are available and when key nutrients are in short supply. This mechanism may allow neuroblastoma cells to continue to grow even in tumor tissues that are deprived of nutrients.

References

1. Medina MA, Sanchez-Jimenez F, Marquez J, et al. (1992) Relevance of glutamine metabolism to tumor cell growth. Mol Cell Biochem 113:1–15
2. Fischer CP, Bode BP, Souba WW (1998) Adaptive alterations in cellular metabolism with malignant transformation. Ann Surg 227:627–636
3. Wasa M, Bode BP, Abcouwer SF, et al. (1996) Glutamine as a regulator of DNA and protein biosynthesis in human solid tumor cell lines. Ann Surg 224:189–197
4. Lusini L, Tripodi SA, Rossi R, et al. (2001) Altered glutathione anti-oxidant metabolism during tumor progression in human renal-cell carcinoma. Int J Cancer 91:55–59
5. Meister A (1991) Glutathione deficiency produced by inhibition of its synthesis, and its reversal; applications in research and therapy. Pharm Ther 51:155–194
6. Carretero J, Obrador E, Anasagasti MJ, et al. (1999) Growth-associated changes in glutathione content correlate with liver metastatic activity of B16 melanoma cells. Clin Exp Metastasis 17:567–574
7. Collins CL, Wasa M, Souba WW, et al. (1998) Determinations of glutamine dependence and utilization by normal and tumor-derived breast cell lines. J Cell Physiol 176:166–178
8. Abcouwer SF, Behrens E, Lustig RJ, et al. (1997) Stress responses to glutamine starvation in human breast cell lines. Proc. Am. Assoc. Cancer Res 38:543
9. Suarez A, Hartmann O, Vassal G, et al. (1991) Treatment of stage IV-S neuroblastoma: a study of 34 cases treated between 1982 and 1987. Med Ped Oncol 19:473–477
10. Gazzola GC, Dall'Asta V, Franchi-Gazzola R, et al. (1981) The cluster tray method for rapid measurement of solute fluxes in adherent cultured cells. Anal Biochem 115:368–374
11. Smith PK, Krohn RI, Hermanson GT, et al. (1985) Measurement of protein using bicinchoninic acid. Anal Biochem 150:76–85
12. Wasa M, Bode BP, Souba WW (1996) Adaptive regulation of amino acid transport in nutrient-deprived human hepatomas. Am J Surg 171:163–169
13. Low SY, Rennie MJ, Taylor PM (1994) Sodium-dependent glutamate transport in cultured rat myotubes after glutamine deprivation. FASEB J 8:127–131
14. Kilberg MS, Han HP, Barber EF, et al. (1985) Adaptive regulation of neutral amino acid transport system A in rat H4 hepatoma cells. J Cell Physiol 122:290–298
15. Wasa M, Wang HS, Tazuke Y, et al. (2001) Insulin-like growth factor-I stimulates amino acid transport in a glutamine-deprived human neuroblastoma cell line. Biochim Biophys Acta 1525:118–124
16. Obrador E, Navarro J, Mompo J, et al. (1997) Glutathione and the rate of cellular proliferation determine tumour cell sensitivity to tumour necrosis factor in vivo. Biochem J 325:183–189
17. Mickisch G, Fajta S, Bier H, et al. (1991) Cross-resistance patterns related to glutathione metabolism in primary human renal cell carcinoma. Urol Res 19:99–103
18. Shotwell MA, Kilberg MS, Oxender DL (1983) The regulation of neutral amino acid transport in mammalian cells. Biochim Biophys Acta 737:267–284

シンポジウム1「周産期・新生児悪性腫瘍」

新生児期に発見された悪性固形腫瘍症例の検討

大阪大学大学院医学系研究科外科学講座（小児成育外科学）[1]，
大阪府立母子保健総合医療センター小児外科[2]，同検査部病理[3]

米田 光宏[1] 大植 孝治[2] 福澤 正洋[1] 草深 竹志[1]
奈良 啓悟[1] 野瀬 聡子[1] 田中 夏美[1] 窪田 昭男[2]
奥山 宏臣[2] 桑江 優子[3] 中山 雅弘[3]

Key words
neonate
malignant solid tumor
neuroblastoma
oncologic emergency

はじめに

新生児期に発症する悪性固形腫瘍は大変稀であるが，しばしばoncologic emergencyを呈し治療に難渋する．新生児悪性固形腫瘍症例の臨床像を明らかにする目的で，大阪大学および大阪府立母子保健総合医療センターにおいて経験した症例について臨床的検討を行った．

対象と方法

大阪大学および大阪府立母子保健総合医療センターにおいて，組織学的に悪性腫瘍と診断された新生児固形腫瘍症例15例を対象とした．

診断は，神経芽腫8例，hemangiopericytoma（HPC）3例，横紋筋肉腫，Rhabdoid tumor of the kidney，副腎皮質癌，infantile fibrosarcomaが各1例ずつであった．

結　果

在胎週数は26週から41週，平均37週で，36週未満は3例であった．出生体重は944gから4,236g，平均2,849gであった．出生前診断は5例（33%）に行われていた．Oncologic emergencyを呈した症例は12例（80%）であった．6例が死亡し，うち5例が発症時にoncologic emergencyを呈していた．死亡原因は，術中死および化学療法の合併症による死亡が各2例，腫瘍破裂によるショック，他病死が各1例ずつであった（表1）．

神経芽腫（表2）

神経芽腫は8例で全体の53%を占めた．INSS病期分類では，stage 4Sが1例，stage 4が4例と遠隔転移を有する症例が半数以上を占めた．8例中7例が来院時oncologic emergencyを呈していた．このうち4例は肝腫大による腹部膨満に起因するものであった．摘出術を施行した4例のうち症例2と3は術後化学療法中に死亡した．摘出術を行わずに救命できたのは3例で，無治療で縮小した症例1，化学療法のみで縮小した症例7，生検後化学療法により縮小した症例8であった．5例が長期生存中で，無治療例を除き，いずれも初期の化学療法を安全に施行し得た症例である．

以下主な症例を呈示する．

症例3は生下時より著明な腹部膨満，呼吸不全を呈し救急搬送された．貧血が進行し，CT上右副腎腫瘍と腹水の貯留，びまん性肝転移を認めた（図1）．腫瘍破裂を来した神経芽腫と診断し，日齢1に右副腎腫瘍摘出術を施行した．術後James療法に準じてVCR 1.0mg/m^2・CPM 200mg/m^{2}を投与したが，真菌感染を合併し，日齢14に死亡した．剖検にて肺転移も確認された．なお本症例の胎盤に異型細胞が認められ，NCAM陽性細胞であることから神経芽腫の胎盤転移と考えられた（図2）．

症例5は生下時より両下肢の運動麻痺，第1腰椎以下の知覚障害と膀胱直腸障害を呈していた．MRIにて右後腹膜腔に腫瘤を認め，第9胸椎から第2腰椎の椎間孔から脊柱管内に腫瘍が進入していた（図3）．Dumb-bell typeの神経芽腫と診断し，半量に減量したJames療法を行った．腫瘍マーカーは低下したが，神経症状は改善しなかったため，日齢55に後腹膜腫瘍摘出及び椎弓切除を行った．またこの際，右胸腔内に胸膜転移を認めたため，stage 4と診断，約半量に減量したA1 protocolを6コース施行した[1]．治療終了後16年経過し，再発なく生存中であるが，下肢麻痺と膀胱直腸障害は残存している．

大阪大学大学院医学系研究科外科学講座（小児成育外科学）
〒565-0871 吹田市山田丘2-2（D6）

Department of Surgery, Division of Pediatric Surgery, Osaka University Graduate School of Medicine,
2-2 Yamadaoka, Suita, Osaka 565-0871, Japan

表1　対象症例

番号	性別	日齢	週数	体重	分娩	診断	原発巣	診断	OE	備考	予後
1	F	0	32	1,298	CS（骨盤位）	院外	後腹膜	神経芽腫	−	経過観察のみ	生存
2	M	7	39	3,200	経膣	院外	後腹膜	神経芽腫	+	術後肝不全，感染	7カ月　死亡
3	F	1	38	3,930	経膣	院外	左副腎	神経芽腫	+	化学療法後腎不全	14日　死亡
4	M	0	40	4,236	経膣	院外	右副腎	神経芽腫	+	挿管，腫瘍破裂	0日　死亡
5	M	15	41	3,800	経膣	院外	後腹膜	神経芽腫	+	膀胱直腸障害	生存
6	F	23	39	3,468	経膣	院外	縦隔	神経芽腫	+	挿管（日齢7），乳糜胸水	生存
7	M	0	38	2,788	経膣	出生前	右副腎	神経芽腫	+	呼吸困難，メレナ	生存
8	F	18	38	2,256	経膣	院外	左頸部	神経芽腫	+	気切	生存
9	F		39	4,004	不明	院外	右上顎	HPC	+	出血，腫瘤	生存
10	M	0	36	2,644	経膣（誘発）	出生前	左肺	HPC	+	挿管，呼吸管理	生存
11	M	0	29	944	CS（徐脈）	出生前	脾臓	HPC	+	腹部膨満	生存
12	F	11	40	2,896	経膣	院外	膣前庭	横紋筋肉腫	−	botryoid type	生存
13	M	0	36	2,870	予定CS	出生前	左頸部	fibrosarcoma	+	高拍出性心不全	7カ月　死亡
14	F	6	26	1,628	経膣	院内	両側副腎	副腎皮質癌	−	EMG症候群，多臓器不全	6日　死亡
15	F	0	39	2,772	経膣	出生前	右腎，小脳	MRTK＋PNET	+	右腎腫瘍破裂にて緊急手術	8日　死亡

日齢：診断日齢，体重：出生体重，CS：帝王切開，HPC：hemangiopericytoma，OE：oncologic emergency

表2　神経芽腫：8例

症例	性別	日齢	診断	原発	病期	OE	治療	備考	予後
1	F	0	院外	後腹膜	1	−	無治療	観察のみで退縮	生存9Y
2	M	7	院外	後腹膜	4	+	OP-C	化学療法後肝不全	死亡（化療）4M
3	F	1	院外	左副腎	4	+	OP-C	化学療法後感染	死亡（化療）14D
4	M	0	院外	右副腎	1	+	蘇生のみ	腫瘍破裂	死亡（ショック）0D
5	M	15	院外	後腹膜	4	+	C-OP-C	Dumb-bell，下肢麻痺	生存16Y
6	F	23	院外	縦隔	4	+	C-OP-C	呼吸困難，乳糜胸水	生存10Y
7	M	7	出生前	右副腎	4S	+	C	呼吸困難，メレナ	生存8Y
8	F	18	院外	左頸部	1	+	B-C	気道確保のため気切	生存2Y

OE：oncologic emergency，OP：手術，C：化学療法，B：生検

図1　神経芽腫（症例3）

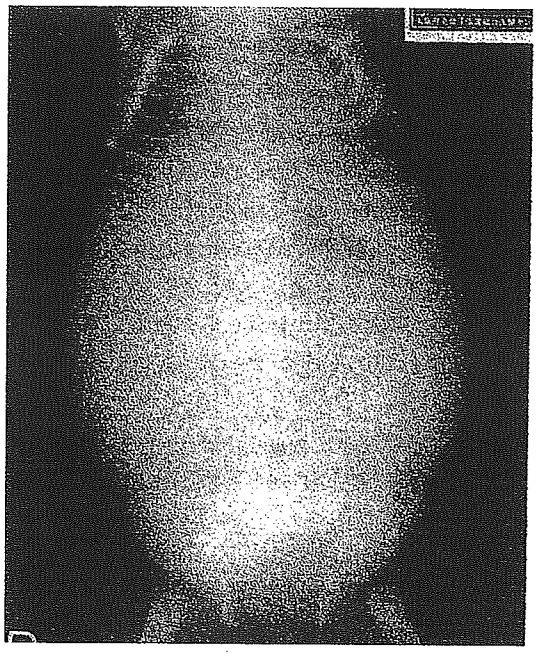

単純X線

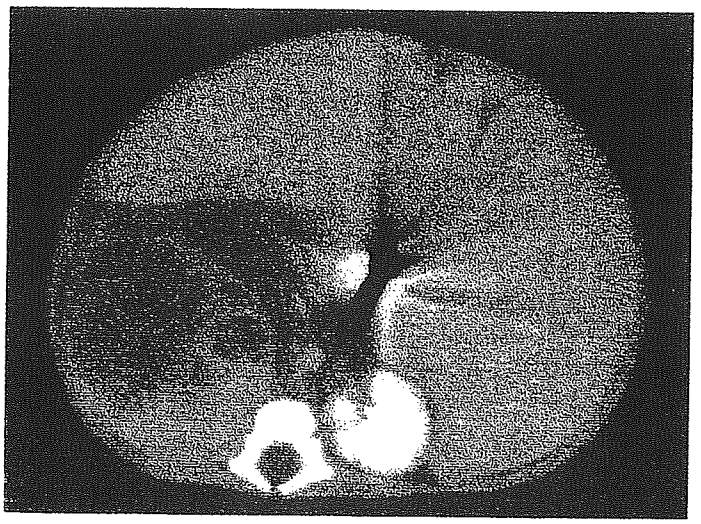

腹部造影CT

図2　胎盤に認められた異型細胞（症例3）

HE染色

NCAM免疫染色

図3　神経芽腫dumb-bell例（症例5：MRI）

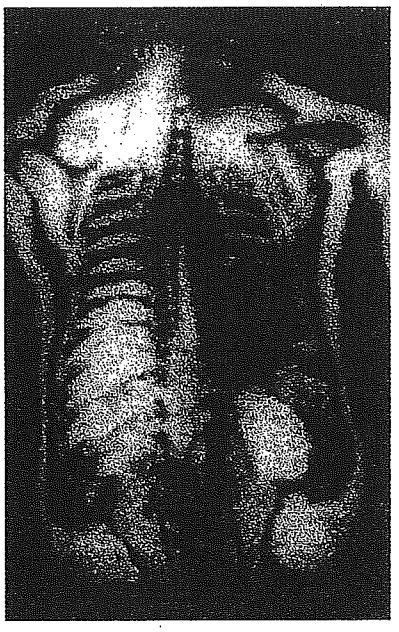

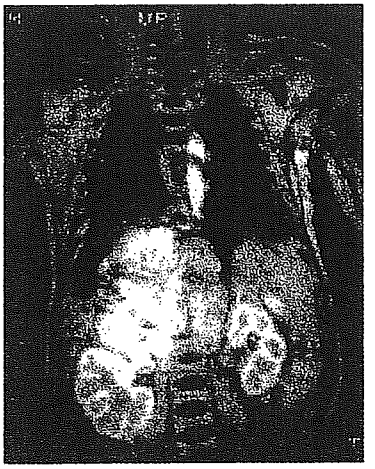

Hemangiopericytoma

Hemangiopericytomaを3例経験した．症例9は右上顎原発例で出血のため治療に難渋した．出生前診断され周産期管理の後，治療された症例が2例あった．症例10は出生前診断により腹腔内の巨大な腫瘤が指摘されていたため，計画分娩の後，生後8時間で緊急手術を行った[2]．症例11も出生前診断例で，妊娠経過中徐脈を認めたため緊急帝王切開を行った．右肺原発腫瘍による呼吸不全を呈したため，生検による診断確定の後，挿管管理下にVCR 0.45mg/m^{2}とCPM 360mg/m^{2}を2コース投与した．CT上腫瘍内造影効果は消失したが，充分な縮小は得られなかったため，日齢69に右中葉を合併切除して腫瘍を摘出した．術後3日間の呼吸管理の後，経過良好で退院した．再発徴候なく生存中である．

横紋筋肉腫

症例12は膣原発のbotryoid type横紋筋肉腫例で，出生時に膣外に発育するブドウ状の腫瘍を認め，生検にて横紋筋肉腫の診断を得，搬送入院となった．手術により腫瘍を全摘し得たため，Group 1と判断し，IRS IIIのプロトコールに従いVAC療法を6コース投与した[3)4)]．治療終了後7年経過しているが再発なく生存中である（図4）．

Infantile fibrosarcoma

症例13は治療に難渋したinfantile fibrosarcoma症例である[5]．26週時の胎児エコーにて頚部腫瘤を指摘され，その後腫瘍内血流の増加と高拍出性心不全徴候を呈したため，36週に帝王切開にて出生．CTおよびMRIにて腫瘍は頸部から縦隔内にも達しており，著明な血

図4　膣原発新生児横紋筋肉腫（症例12）

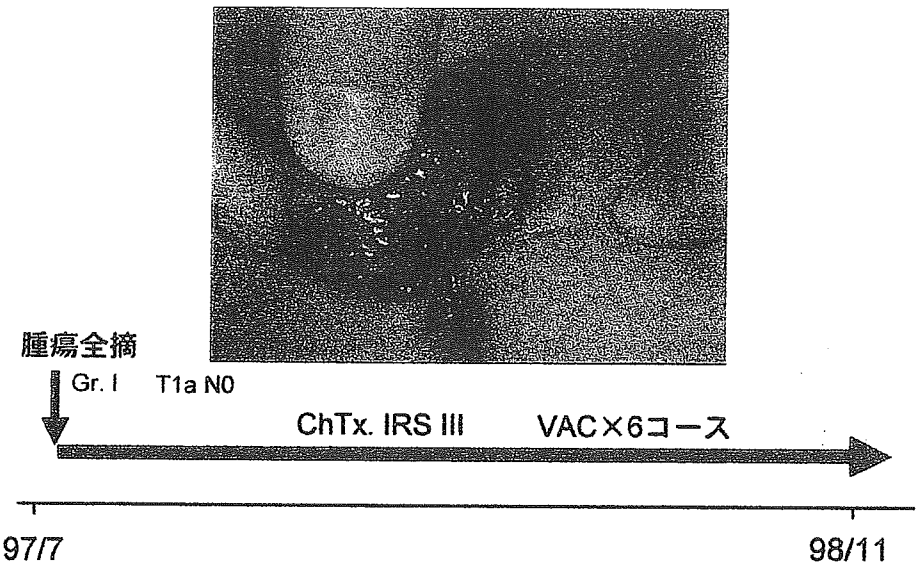

図5　Infantile fibrosarcoma（症例13）

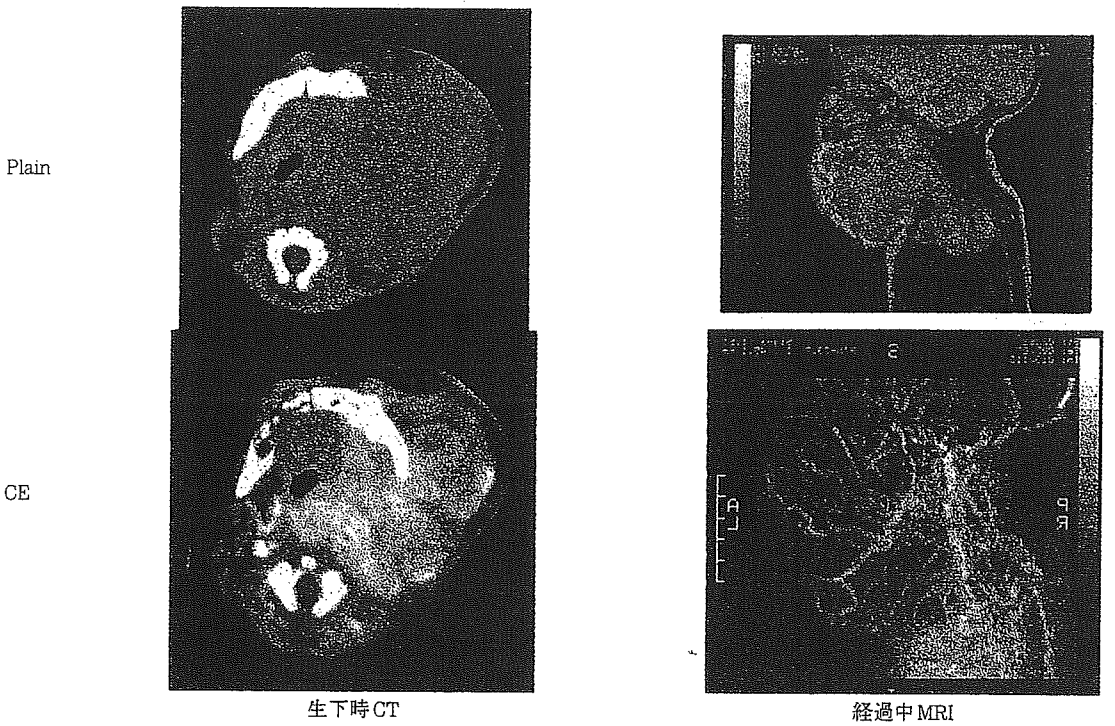

管増生が見られた（図5）．当初は血管腫と診断し，ステロイド，アスピリン，CPM投与を行ったが，徐々に腫瘍は増大し，人工呼吸管理を要するようになった．放射線療法も奏効せず，その後高カルシウム血症も合併したため，開胸手術を敢行したが術中出血により死亡した．剖検後の組織診断にてinfantile fibrosarcomaの最終診断を得た．

副腎皮質癌[6) 7)]

症例14はEMG症候群を合併した副腎皮質癌の症例である．25週の胎児エコーで羊水過多と臍帯ヘルニアを指摘され，高位破水を来したため，26週で頚腟分娩．生下時体重1,628g，胎児水腫を認めた．また臍帯ヘルニアに加え，巨舌もみられたことからEMG症候群と診断した．腎不全，心不全を併発し，日齢6に死亡．剖

図6 副腎皮質癌症例（EMG症候群合併：症例14）

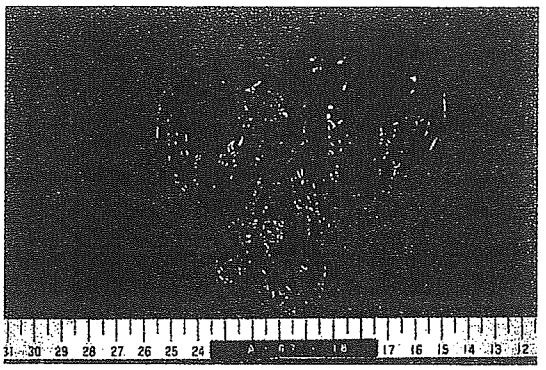
右副腎腫瘍

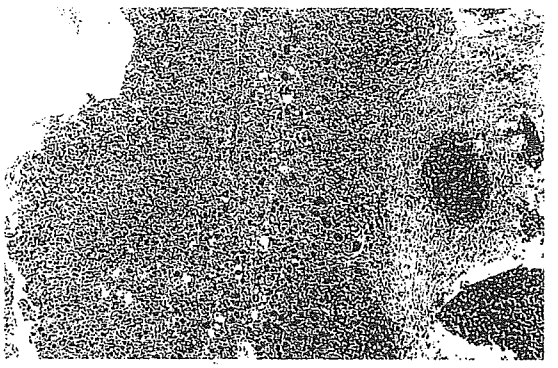
副腎：低倍

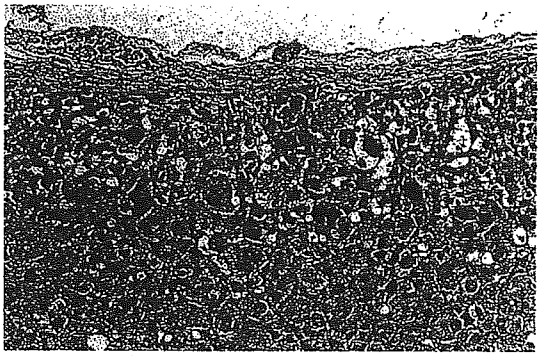
副腎：高倍

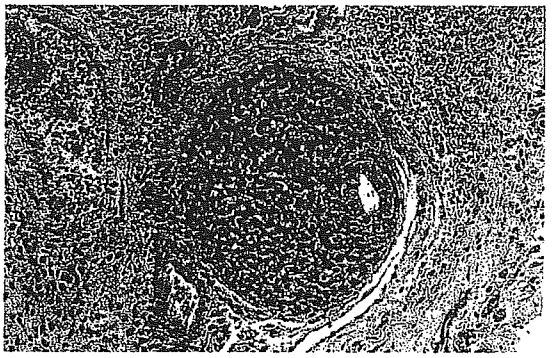
卵巣転移

図7 *INI1*遺伝子のPCR-SSCP（exon 9）（症例15）

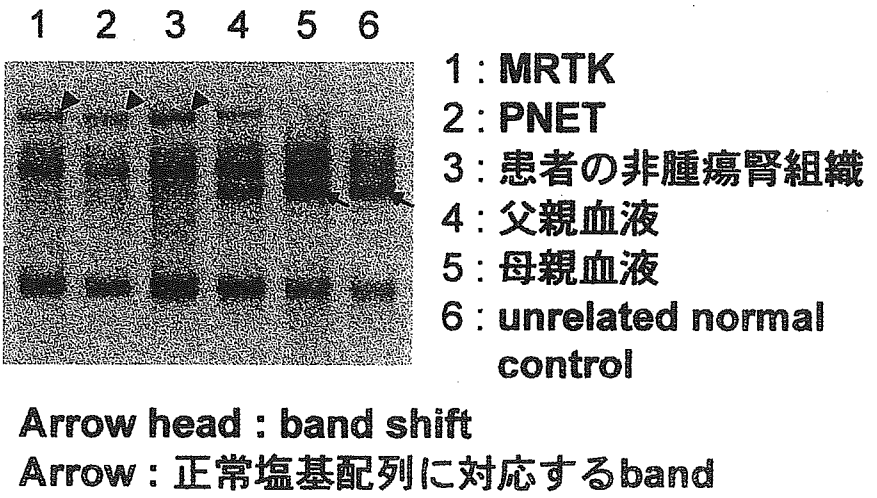

検により両側副腎に腫瘍を認め，副腎皮質癌と診断された．また，肺，卵巣に複数の転移巣を認めた（図6）．

MRTK・小脳PNET合併例[8]

症例15は出生当日に右腎腫瘍破裂による腹腔内出血にて発症．緊急右腎摘出術を行い，組織学的にMRTKの診断を得た．同時に小脳腫瘍を認め，日齢7に開頭術を行ったが，術中出血により死亡した．小脳腫瘍はPNETの診断であった．RTKと中枢性PNET（cPNET）の合併には*INI1*遺伝子変異が関与していることが判明しているため[9,10]，両親の承諾を得て*INI1*遺伝子変異の検索を行った．SSCP法により検討すると，exon 9に異常が認められた（図7）．レーン1，2の腫瘍組織，3の非腫瘍組織のみならず，患児の父親に特徴的なバンドが認められた．これはpolymorpismに起因しており，レーン5，6の母親と正常コントロールのパターンと比較すると，父親ではwild typeとpolymorphismのheterozygosityを示した．患児の組織では非腫瘍組織も含めてpolymorphismのパターンのみが認められ，患児

においては母親由来の*INI1*遺伝子がgerm-lineで欠失していることが判明した（図7）．次に*INI1*遺伝子座の存在する22番染色体長腕上のマイクロサテライトマーカーを用いて検索すると，患児のMRTK，PNETいずれにおいても，非常に大きな領域のLOHが確認された．両腫瘍における*INI1*遺伝子発現がほとんど検出されないという傍証も得たことから，患児はgermlineで母親由来の*INI1*遺伝子が欠失しており，さらに両腫瘍内において，残された父親由来の遺伝子も欠失していると結論した[8]．

考　察

新生児悪性固形腫瘍症例15例中12例（80%）が腫瘍に起因する緊急症状，いわゆるoncologic emergencyを呈していた．全身管理の難しい新生児期に重篤な症状を呈する症例は予後不良で，12例中5例が死亡している．Oncologic emergencyの症状は，腹部膨満，気道圧迫や胸水による呼吸障害，腫瘍破裂による出血性ショックが複数例に見られた．その他dumb-bell型神経芽腫に生じた神経障害，血管腫様の高拍出性心不全症状を呈した巨大頸部fibrosarcomaも特徴的であった．

胎内や出生直後に重篤な症状を呈する症例では，出生前診断に基づく計画的な周産期管理が大切である．大阪府立母子保健総合医療センターにおいて胎児診断された腫瘤性病変を検討した大槌ら[11]によると，管理上の問題点として，1）腫瘤が巨大で産道通過障害を来す可能性がある場合，2）腫瘤が急速に増大する場合，3）腫瘍出血や高拍出性心不全による胎児の状態が不良となる場合，4）気道圧迫などにより出生後に緊急蘇生処置が必要となる場合，を挙げている．これらに対応した周産期管理が治療成績向上のために重要であると考えられる．

疾患別では，神経芽腫が8例と最多であった．このうち問題となったのは，びまん性肝転移を有し，著明な肝腫大から呼吸不全を呈する症例である．救命は極めて困難で，早期に適切な放射線療法や化学療法を行うことが推奨される．このためには早期診断が重要であるが，全身状態が悪く開腹生検が不可能な症例では，症例3のように胎盤の腫瘍細胞を確認することも早期診断の一助となろう．次に問題となるのは下肢麻痺や膀胱直腸障害をもたらすdumb-bell型神経芽腫症例である．一般的に腫瘍の生命予後は良好であるが神経症状を残す症例が多い．以前は緊急椎弓切除を行い，圧迫を解除することが行われてきたが，側彎等の晩期障害を来すことが問題である．胎児期から長期間脊髄圧迫を受けていた症例では，椎弓切除を行っても神経症状の改善が期待できない．神経芽腫は化学療法に対する反応も良いので，最近は化学療法を優先させることが推奨されている[12]．

新生児神経芽腫の場合，*MYCN*増幅の見られた症例は極めて稀で，多くの症例において生物学的予後因子は良好である[13]．重篤なoncologic emergencyを呈した症例6，7，8においても，適切な化学療法を行えば腫瘍の縮小は極めて良好で，いずれも救命できている．反面，腫瘍破裂を来した症例4と化学療法による重篤な合併症を来した症例2，3を失った．特に臓器機能が未熟な新生児に対する化学療法は，重篤な合併症を生じることが多いため，薬剤，用量の選択が重要である．

Hemangiopericytomaは1歳以上の患児に好発するadult typeと1歳未満に見られるinfantile typeに大別される．前者は成人例と同様予後不良で，積極的な集学的治療が必要とされる．一方，新生児症例を含むinfantile typeはinfantile myofibromatosisと同じスペクトラムにある腫瘍とされ[14][15]，自然退縮も期待できることから，過剰な治療は慎むべきである[16][17]．しかしながら新生児期に巨大腫瘤による圧迫症状を来すこともあり，慎重な周産期管理を要する．症例10および11において，産科と協力して胎児期からの管理を行うことで良好な結果を得た[2]．また，症例10において腫瘍の縮小を期待して化学療法を施行した．充分な縮小効果は得られなかったものの，腫瘍内の造影効果が減弱するなどの変化が見られた．近年infantile typeは化学療法に対する反応が良好であるという報告も出ている[16][17]．

膣原発の新生児横紋筋肉腫例に対しては全摘後にIRS Ⅲに準じて化学療法を行った[3][4]．1歳以下の乳児例に対する化学療法は減量して行うべきという報告が多く[18][19]，特に3カ月未満の患児に対してはアントラサイクリン系の抗癌剤投与は行うべきでないという意見がある[18]．本症例では安全に治療を遂行できたが，今後は慎重に治療法を選択する必要があり，グループスタディによる多数例での検討が待たれる．

Infantile fibrosarcoma例は不幸な転帰をとった．出生前に血流の豊富な腫瘤性病変がとらえられていたが，当初は血管腫と考えていたために，自然退縮を期待した姑息的治療に終始した．臨床経過が典型的でない場合は悪性腫瘍も念頭に置いて，生検による正確な診断を行い，早期から集学的治療を行うべきであったと反省される．

副腎皮質癌は，生後6時間で他病死したEMG症候群症例の剖検時に発見されたものである．多数例の検討では，EMG症候群の約8.5%に悪性腫瘍の合併が見られるとされる[20]．副腎皮質癌の合併はWilms腫瘍に次いで多く，11p15.5のLOHや*IGF2*遺伝子の発現亢進が両疾患に共通して観察されることから，共通する遺伝子異常がその病因であることが明らかとなってきた[21]．本症例はgermlineに11番染色体短腕上でgenomic imprintingを主体とした遺伝子異常を来し，これが副腎皮質癌の胎児期発生，多発性転移に関与したと考えられた．

MRTKとcPNETのいずれも，胎児期に発生するのは極めて稀である．患児と両親の遺伝子検索により，患児はgermlineで母親由来の*INI1*遺伝子が欠失しており，さらに両腫瘍内において，残された父親由来の遺伝子も欠失していることが判明した．近年両疾患の合併例では，本例と同様に，一方のalleleの*INI1*遺伝子変異がgermlineで存在し，それぞれの腫瘍内でもう一方のalleleに変異を生じていることが観察されている[9,10,22]．

先に示した副腎皮質癌症例と同様，germlineにおける遺伝子変化が胎児期の腫瘍形成に重要な役割を果たしていることを示唆する症例であった．副腎皮質癌，MRTKとも極めて悪性度の高い難治性疾患で，遺伝子変化に着目した新たな治療法の開発が期待される．

まとめ

新生児期に発見された悪性固形腫瘍15例を検討した．

12例80%がoncologic emergencyを呈しており，うち5例が死亡していた．

15例中8例は神経芽腫で，化学療法に反応した4例と自然退縮した1例が生存中である．死亡3例中2例は合併症死しており，新生児の治療法の選択が重要であると思われた．

またgermlineに遺伝子異常を有する例が2例存在した．

稀な新生児悪性固形腫瘍の治療成績改善のためには，多施設で症例を集積し検討する必要があると思われた．

文　献

1) 米田光宏，福沢正洋，草深竹志，ほか．新生児Dumb-bell型神経芽腫の1例．小児がん　1990；27：349-51
2) 田中夏美，窪田昭男，川原央好，ほか．胎児超音波検査にて発見された超低出生体重児の脾臓原発血管外皮腫の1治験例．日本小児外科学会雑誌　2005；41：206-11.
3) Crist WM, Anderson JR, Meza JL, et al. Intergroup rhabdomyosarcoma study-IV: results for patients with nonmetastatic disease. J Clin Oncol 2001；19：3091-102
4) Crist W, Gehan EA, Ragab AH, et al. The Third Intergroup Rhabdomyosarcoma Study. J Clin Oncol 1995；13：610-30
5) 米田光宏，井村賢治，八木　誠．腫瘍と電解質代謝異常．小児外科1995；27：1405-12
6) Nakayama M, Kubota A. A case of adreno-cortical tumor in a premature baby with EMG syndrome. Arch Histopathol D D 2004；11：16-9
7) 福澤正洋，川原央好，草深竹志，ほか．出生後早期に多発転移を認めたEMG症候群合併，副腎皮質癌の1例．小児がん　1988；25：549-51
8) Kusafuka T, Miao J, Yoneda A, et al. Novel germ-line deletion of SNF5/INI1/SMARCB1 gene in neonate presenting with congenital malignant rhabdoid tumor of kidney and brain primitive neuroectodermal tumor. Genes Chromosomes Cancer 2004；40：133-9
9) Versteege I, Sevenet N, Lange J, et al. Truncating mutations of hSNF5/INI1 in aggressive paediatric cancer. Nature 1998；394：203-6
10) Savla J, Chen TT, Schneider NR, et al. Mutations of the hSNF5/INI1 gene in renal rhabdoid tumors with second primary brain tumors. J Natl Cancer Inst 2000；92：648-50
11) 大植孝治，窪田昭男，川原央好，ほか．出生前診断された腫瘤性病変の治療方針．小児がん　2004；41：805-9
12) Bernardi BD, Balwierz W, Bejent J, et al. Epidural compression in neuroblastoma: Diagnostic and therapeutic aspects. Cancer Lett 2005；228：283-99
13) Granata C, Fagnani AM, Gambini C, et al. Features and outcome of neuroblastoma detected before birth. J Pediatr Surg 2000；35：88-91
14) Mentzel T, Calonje E, Nascimento AG, et al. Infantile hemangiopericytoma versus infantile myofibromatosis. Study of a series suggesting a continuous spectrum of infantile myofibroblastic lesions. Am J Surg Pathol 1994；18：922-30
15) Variend S, Bax NM and van Gorp J. Are infantile myofibromatosis, congenital fibrosarcoma and congenital haemangiopericytoma histogenetically related? Histopathology 1995；26：57-62
16) Ferrari A, Casanova M, Bisogno G, et al. Hemangiopericytoma in pediatric ages: a report from the Italian and German Soft Tissue Sarcoma Cooperative Group. Cancer 2001；92：2692-8
17) Rodriguez-Galindo C, Ramsey K, Jenkins JJ, et al. Hemangiopericytoma in children and infants. Cancer 2000；88：198-204
18) Ferrari A, Casanova M, Bisogno G, et al. Rhabdomyosarcoma in infants younger than one year old: a report from the Italian Cooperative Group. Cancer 2003；97：2597-604
19) Ragab AH, Heyn R, Tefft M, et al. Infants younger than 1 year of age with rhabdomyosarcoma. Cancer 1986；58：2606-10
20) Sotelo-Avila C, Gonzalez-Crussi F, Starling KA. Wilms' tumor in a patient with an incomplete form of Beckwith-Wiedemann syndrome. Pediatrics 1980；66：121-3
21) Steenman M, Westerveld A, Mannens M. Genetics of Beckwith-Wiedemann syndrome-associated tumors：common genetic pathways. Genes Chromosomes Cancer 2000；28：1-13
22) Biegel JA, Zhou JY, Rorke LB, et al. Germ-line and acquired mutations of INI1 in atypical teratoid and rhabdoid tumors. Cancer Res 1999；59：74-9

Available online at www.sciencedirect.com
SCIENCE DIRECT®
ELSEVIER
Health Policy 73 (2005) 52–57
HEALTH POLICY
www.elsevier.com/locate/healthpol

Actual and estimated costs of disposable materials used during surgical procedures

Shin-ichi Toyabe[a,*], Pengyu Cao[a], Sachiko Kurashima[a], Yukiko Nakayama[b], Yuko Ishii[b], Noriko Hosoyama[b], Kouhei Akazawa[a]

[a] *Department of Medical Informatics, Niigata University Medical and Dental Hospital, Asahimachi-dori 1-754, Niigata 951-8520, Japan*
[b] *Operating Department, Niigata University Medical and Dental Hospital, Niigata, Japan*

Abstract

It is difficult to estimate precisely the costs of disposable materials used during surgical operations. To evaluate the actual costs of disposable materials, we calculated the actual costs of disposable materials used in 59 operations by taking account of costs of all disposable materials used for each operation. The costs of the disposable materials varied significantly from operation to operation (US$ 38–4230 per operation), and the median [25-percentile and 75-percentile] of the sum total of disposable material costs of a single operation was found to be US$ 686 [205 and 993]. Multiple regression analysis with a stepwise regression method showed that costs of disposable materials significantly correlated only with operation time ($p < 0.001$). Based on the results, we propose a simple method for estimating costs of disposable materials by measuring operation time, and we found that the method gives reliable results. Since costs of disposable materials used during surgical operations are considerable, precise estimation of the costs is essential for hospital cost accounting. Our method should be useful for planning hospital administration strategies.

Keywords: Hospital resources; Cost sharing

1. Introduction

Since many kinds of disposable materials are used during operations, it is difficult to estimate precisely the costs of these materials [1,2]. The costs of disposable materials such as gauzes, needles and strings, which are used in large numbers, are particularly difficult to calculate. The costs of these disposable materials are usually allocated to operations from total costs of disposable materials used in the operation department [3]. However, this method is based on the incorrect assumption that the same amounts of disposable materials are used during operation regardless of the kind of operation.

The objective of this study was to evaluate the precise costs of disposable materials used during operations and to develop a method to estimate precisely the costs of disposable materials used during an operation. To calculate actual costs of disposable materials used during each operation, we recorded lists of all

* Corresponding author. Tel.: +81 25 227 2472; fax: +81 25 227 0850.
E-mail address: toyabe@med.niigata-u.ac.jp (S.-i. Toyabe).

0168-8510/$ – see front matter © 2004 Elsevier Ireland Ltd. All rights reserved.
doi:10.1016/j.healthpol.2004.10.003

disposable materials used during the operation. The results showed that the costs of disposable materials varied from operation to operation and that the total cost of disposable materials is considerable. Although this method gives precise results, it is too time-consuming [1,2,4]. A more practical method is needed for calculation of material costs of each operation [5,6]. We developed a more practical method to calculate costs of medical materials used during operations [3,7].

2. Materials and methods

A flowchart of the method of analysis used in this study is shown in Fig. 1. The analysis was divided into three steps: collection of cost data, identification of cost allocation factors, and comparison of actual costs with estimated costs. Each of these steps is explained in detail below.

2.1. Collection of cost-related data

Cost-related data for the eleven factors in step 1 in Fig. 1 were collected in 59 operations during the period from July to October in 2003. The 11 factors were (1) patient background, (2) operation method, (3) disposable material costs, (4) number of disposable materials, (5) operation time, (6) number of staff and (7) anesthesia method. Table 1 shows the surgical procedures used.

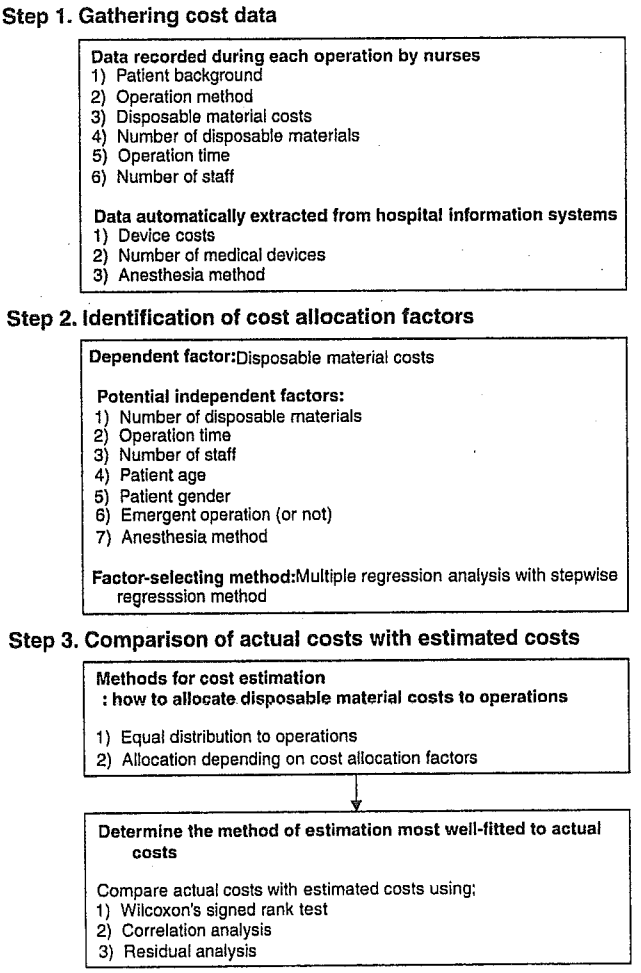

Fig. 1. Analysis flowchart.

Table 1
List of surgical procedures

Operation	Number of cases
Bilateral pediatric inguinal herniotomy	1
Cataract operations plus intraocular lens inplantation	3
Cerebral revasculization	2
Glaucoma operation (goniotomy) plus intraocular lens inplantation	2
Glaucoma operation (trabeculectomy)	2
Glaucoma operation (trabeculectomy) plus intraocular lens inplantation	1
Heart valve replacement	3
Hepatic segmentectomy	2
Laparoscopic adnexectomy	3
Lobar hepatectomy	1
Pediatric inguinal herniotomy plus hydrocelectomy	1
Pediatric inguinal herniotomy plus umbilical herniotomy	2
Renal transplantation	3
Renal transplantation and splenectomy	1
Replacement of artificial hip joint	1
Replacement of artificial hip joint plus autologous bone transplantation	2
Resection of pancreas head	1
Resection of pancreas head plus arterioplasty	1
Resection of rectal cancer	2
Resection of rectal cancer plus cholecystectomy	1
Strabismus surgery	2
Thoracoscopic lobectomy	3
Total colectomy	2
Total gastrectomy	5
Transurethral prostate biopsy	2
Tympanoplasty	2
Unilateral pediatric inguinal herniotomy	2
Vitreous surgery	1
Vitreous surgery plus intraocular lens inplantation	5
Total	59

To obtain actual cost data, we made a list of all of the medical materials, including materials of low cost such as sheets of gauze, used during each operation. All medical materials used during each operation were recorded by a nurse who did not attend the operation. The number of medical staff who attended the operation, including doctors, nurses and medical engineers, was also recorded. The cost of each disposable material was calculated by adding the price of the material to the cost of maintaining the material handling department. The price data of each material was based on the database supplied University Hospital Medical Information Network (UMIN) [8]. The total costs of maintaining the material handling department were allocated to each material according to the price of the material. Grubbs-Smirnov test was used to detect outliers in the distribution of cost data [9].

2.2. Identification of cost allocation factors

"Cost allocation factors" are allocation bases utilized for applying costs to services or procedures, resembling cost drivers used in an activity-based costing (ABC) system [7]. We selected cost allocation factors from factors that significantly affect disposable material costs (number of disposable materials, operation time, number of staff, patient age, gender, anesthesia method, emergency operation or not) using multiple regression analysis with a stepwise regression method [10]. All variables were standardized to zero mean and unit variance. The significance level of 0.05 was adopted as the criterion for entering the factors into the regression model, regarding the stepwise method. Univariate regression analysis was performed to study association between cost of disposable materials and each of the factors listed above.

2.3. Comparison of actual costs and estimated costs

Generally, cost data of all disposable materials used in an operating room are easily obtained from the hospital information systems. To calculate the disposable material costs in a single operation, the total costs should be distributed to operations in an appropriate manner. The conventional method to allocate total costs of disposable materials to operations is equal distribution to operations [3]. We propose an alternative method: allocation of total costs to each operation based on predetermined cost allocation factors. Wilcoxon's signed rank test was used to compare the actual cost data and the estimated cost data. A p-value of less than 0.05 was considered statistically significant. The 'goodness of fit' in each estimation was analyzed by the coefficient of determination and residuals between estimated costs and actual costs. All cost data are expressed in US dollars. The distributions of continuous data were expressed by median [25-percentile

and 75-percentile] or by mean ± standard deviation if appropriate.

3. Results

3.1. Actual cost data of medical materials used during operations

The actual costs of all disposable materials varied from US$ 38 to US$ 4230, and the median [25-percentile and 75-percentile] cost was US$ 686 [205 and 993]. The number of disposable materials used during an operation differed from 17 to 697, the median [25-percentile and 75-percentile] being 80 [57,165].

3.2. Variances of costs of the same operation

Variances of costs of medical materials in total gastrectomies performed on five patients were examined. The operations were performed by different surgeons, but the patients' backgrounds are the same. The costs of disposable materials used in each operation varied from US$ 948 to US$ 5825 (median, US$ 2875).

3.3. Regression analysis of costs of disposable materials

Multiple regression analysis was performed by the stepwise regression method to determine the importance of factors associated with disposable material costs [10]. Operation time was the only factor selected as a significant factor associated with disposable material costs (standardized correlation coefficient of 0.927, $p < 0.001$). Univariate regression analysis showed that operation time was significantly associated with disposable material cost ($R^2 = 0.859$, $p < 0.001$).

3.4. Average costs of disposable materials per unit of operation time and per operation

Since disposable material costs were found to depend on operation time, we calculated the average cost per unit of operation time (Fig. 2). The costs per unit of operation time were almost constant in all but two operations. The costs of those two operations were much higher than those for other operations and were shown to be outliers by the Grubbs-Smirnov test ($p < 0.01$) [9]. They were cataract operations plus intraocular lens implantation, and the reason for the high costs of these operations is the high costs of intraocular lenses. The disposable material cost per operation time was US$ 3.2/min [2.2, 3.9] based on data for 57 operations, whereas it was US$ 3.70/min calculated by total costs and sum of operation times for the operations performed in the operating room in our hospital in 2003. The disposable material cost per operation was calculated to be US$ 459.3.

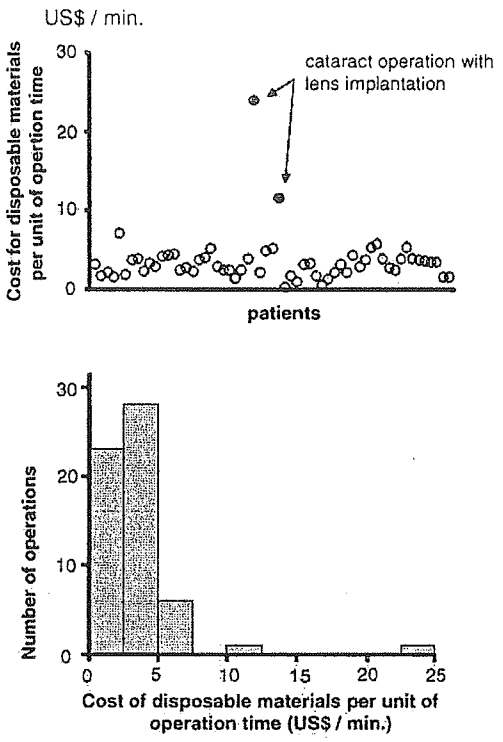

Fig. 2. Disposable material costs per unit of operation time in each operation. Two operations were shown to be outliers by the Grubbs-Smirnov test ($p < 0.01$, closed circles).

3.5. Estimated costs of medical materials used during each operation

Based on the results of multiple regression tests, we estimated costs of disposable materials by allocating to each operation equally (conventional method) and by allocating to each operation according to operation time. The costs estimated by these methods were compared with the actual costs in 57 operations (Table 2). The actual costs were significantly different from the

Table 2
Comparison of costs of disposable medical materials used during operations estimated by two different methods

Methods for estimation of cost of disposable materials	Comparison with actual cost (p)[a]	Coefficient of determination (R^2)[b]	Residual between estimated and actual costs[c]
1. Equal distribution to operation	0.001	–	−365.2 ± 814.5
2. Cost allocation in proportion to operation time	0.062	0.927 ($p < 0.001$)	88.6 ± 306.3

[a] Wilcoxon's signed rank test was used to examine differences between actual costs and estimated costs.
[b] Pearson's correlation test was used to examine correlation between actual costs and estimated costs.
[c] Residual between estimated costs and actual costs is expressed as mean ± S.D.

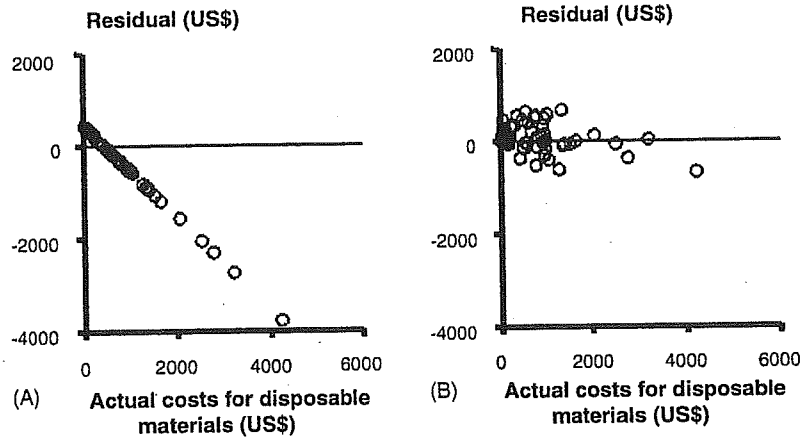

Fig. 3. Relationship between the actual costs of disposable materials used during operations and the residuals that were estimated costs minus actual costs. The estimated costs were calculated by the conventional method, in which costs were allocated equally to operations (A), and by our method, in which costs were allocated to operations according to operation time (B).

costs estimated by the conventional method ($p = 0.001$). The costs estimated by our method, on the other hand, agreed well with the actual costs. The average residual between the actual costs and the costs estimated by our method was smaller than that estimated by the conventional method (Fig. 3).

4. Discussion

Current status of disposable material costs is not obvious, because it is not exactly known what materials are used for an individual patient [11,12]. Our results demonstrate that the disposable material costs per operation are considerable and vary significantly from operation to operation. Therefore, precise calculation of disposable materials used for each operation is essential to know the precise costs per operation and to reduce variance between physicians [1,13]. Inappropriate allocation of disposable material costs would result in the adoption of erroneous strategies for hospital management.

Since calculation of disposable material costs by adding the costs of all materials is a precise but time-consuming method [1], other methods to allocate total costs of disposable materials to operations are needed [3,6,7,14,15]. The costs of disposable materials have been calculated by allocating the costs equally to operations. However, our results demonstrate that cost data estimated by the conventional method differ significantly from actual cost data (Table 2). We determined the factors that significantly affect costs of disposable materials by using multiple regression analysis to ascertain the cost allocation factors. The results revealed that the only factor regressed with disposable material costs was operation time. We therefore proposed a simple method for estimating the costs of each operation based on regression using operation time as an

explanatory variable. Our method for estimating costs of disposable materials is simple, more reliable than previous methods, and applicable to most operations except for some outliers (Fig. 2). Our method should be useful for planning hospital administration strategies.

References

[1] Allen JW, Polk Jr HC. A study of added costs of laparoscopic cholecystectomy based on surgery preference cards. The American Surgeon 2002;68:474–6.

[2] Adachi Y, Shiraishi N, Ikebe K, Aramaki M, Bandoh T, Kitano S. Evaluation of the cost for laparoscopic-assisted Billroth I gastrectomy. Surgical Endoscopy 2001;15:932–6.

[3] Udpa S. Activity cost analysis: a tool to cost medical services and improve quality of care. Management Care Quarterly 2001;9:34–41.

[4] Udpa S. Activity-based costing for hospitals. Health Care Management Review 1996;21:83–96.

[5] Austin PC, Ghali WA, Tu JV. A comparison of several regression models for analysing cost of CABG surgery. Statistics in Medicine 2003;22:2799–815.

[6] West TD, Balas EA, West DA. Contrasting RCC, RVU, and ABC for managed care decisions. A case study compares three widely used costing methods and finds one superior. Healthcare Finance Management 1996;50:54–61.

[7] Baker JJ, Boyd GF. Activity-based costing in the operating room at Valley View Hospital. Journal of Health Care Finance 1997;24:1–9.

[8] UMIN. See http://www.umin.ac.jp/practice/pharmaceuticals/ (in Japanese). Last checked September 20, 2004.

[9] Stefansky W. Rejecting outliers in factorial designs. Technometrics 1972:14469–79.

[10] Johnson RA, Wichern DW. Applied multivariate statistical analysis. Englewood Cliffs, NJ: Prentice Hall; 1992.

[11] Bertges DJ, Zwolak RM, Deaton DH, Teigen C, Tapper S, Koslow AR, et al. Current hospital costs and medicare reimbursement for endovascular abdominal aortic aneurysm repair. Journal of Vascular Surgery 2003;37:272–9.

[12] Oliver A. Health economic evaluation in Japan: a case study of one aspect of health technology assessment. Health Policy 2003;63:197–204.

[13] Welcker K, Marian P, Thetter O, Siebeck M. Cost and quality of life in thoracic surgery—a health economic analysis in a German center. Thoracic and Cardiovascular Surgery 2003;51:260–6.

[14] Lievens Y, van den Bogaert W, Kesteloot K. Activity-based costing: a practical model for cost calculation in radiotherapy. International Journal of Radiation Oncology, Biology, Physics 2003;57:522–35.

[15] DesHarnais Castel L, Bajwa K, Markle JP, Timbie JW, Zacker C, Schulman KA. A microcosting analysis of zoledronic acid and pamidronate therapy in patients with metastatic bone disease. Support Care Cancer 2001;9:545–51.

Hiroshima J. Med. Sci.
Vol. 54, No. 1, 9~20, March, 2005
HIJM 54–2

Multi-target Models and their Application to Data Analysis of Cellular Mortality due to Radiation Exposure

I Made ARCANA[1)] and Megu OHTAKI[2)]

1) Graduate School of Biomedical Sciences, Hiroshima University, 1–2–3 Kasumi, Minami-ku, Hiroshima 734–8551, Japan

2) Department of Environmetrics and Biometrics, Research Institute for Radiation Biology and Medicine, Hiroshima University, 1–2–3 Kasumi, Minami-ku, Hiroshima 734–8551

ABSTRACT

We consider multi-target models for use in analyzing data of the dose-response relationship. The target sizes we are concerned with here are both homogeneous, as assumed in the classical model, and heterogeneous, as simplified using geometric progression. We apply two models for establishing the multi-target models: a Poisson regression model constructed by assuming that the response variable Y follows Poisson distribution, and a gamma-frailty model as a Poisson mixture model derived by adding random common risks having a gamma distribution. Applying these models to experimental data relating the effects of miso fermentation-stages on the survival rate of cells of intestinal crypts of mice exposed to radiation yielded the result that there were substantial frailties associated with all miso fermentation-stages. Short-term and medium-term fermented miso provided similar effects, whereas long-term fermentation had the lowest relative risk value, indicating a significant protection of the crypts against exposure effects. A gamma-frailty model based on heterogeneous target size was more suitably applied when there were at least 3 dead stem cells having 10 target genes.

Key words: *Gamma-frailty model, Miso (fermented soy bean paste), Poisson regression model, Radio protective effects*

For more than fifty years, the multi-stage model proposed by Armitage and Doll[1)] has continued to influence biomedical thinking on cellular changes, particularly in regard to the processes underlying carcinogenesis (e.g., see 2, 15, 17, 21, and 23). This model, however, is derived according to a probabilistic mechanism that is precisely described on the basis of reasonable assumptions[23)], of which correspondence to actual events in biomedical fields has not been established. Therefore, Moolgavkar[15)] noted that the multi-stage model needs to be embellished in various ways to accommodate our current thinking on carcinogenesis.

Building on the idea of removing stages from the multi-stage model of cell changes, the purpose of the present paper is to establish mathematical models for examining the relation of the dose response level of exposure to cellular changes on the pathway to cell death. These dose-response-based models, called multi-target models, consider a unit in exposed cells as a target.

Survival curves for most mammalian cells exposed to low-LET radiation, such as gamma and X-rays, show a shoulder-shaped curvature, in which there is less cell inactivation per unit dose at the initial low dose region and a tendency towards a constant slope at the higher dose. This constant final slope is caused by the effect of the repair of DNA single strand breaks during exposure. The shoulder region of the curve can be interpreted in two possible ways. Firstly, the given dose is considered as a total of dose fractions that are individually capable of repairing sub-lethal damage in between them[15)], but become lethal damage when added together. In this situation, we assume that each dose fraction is given acutely and that the repair of the single strand breaks during the radiation can be ignored. Secondly, lesions are individually reparable, but when the efficiency of the enzymatic repair mechanisms diminishes due to the number of lesions, they are become irreparable and kill the cell. This means that it requires more than two targets getting exposure to radiation on the pathway to cell death. For these reasons, we applied multi-target models to cellular mortality due to radiation exposure.

Suppose that the probability of a target surviving after exposure at dose D is expressed by the survival function $S(D\,|\,\beta)=e^{-\beta D}$, where β is an unknown parameter describing the coefficient of exposure effects. Under such a condition, the probability of a target having vital damage is denoted by the failure distribution[12)] $F(D\,|\,\beta)=1-e^{-\beta D}$. In the classical multi-target model, it is assumed that

lethal damage occurs after independent hits on a certain number of targets (say k), and that the target size is homogeneous. Here, the target size is related to its sensitivity level to radiation effects. The larger the target sizes the higher probability of it getting hit when exposed to radiation. The target survivor function is thus

$$S_k(D|\beta) = 1 - (1 - e^{-\beta D})^k. \quad (1)$$

However, the assumption of homogeneous target size is sometimes unrealistic. It is therefore appropriate to remove this assumption. A general extension of the target survivor function shown in equation (1) that allows each hit target to have a different exposure effect can be formulated by

$$S_k(D|\beta_1, \ldots, \beta_k) = 1 - \prod_{j=1}^{k}(1 - e^{-\beta_j D}), \quad (2)$$

where (unknown) parameter β_j represents the coefficient of sensitivity for the j-th target, j=1, 2, ... , k.

For establishing the multi-target models, we apply two models: a Poisson regression model constructed by assuming that the response variable Y follows Poisson distribution, and a gamma-frailty model as a Poisson mixture model derived by adding random common risks having a gamma distribution.

MULTI-TARGET MODELS

1. Geometric Structure on Heterogeneous Targets

By assuming that the parameter of the sensitivity coefficient for the j-th target (β_j) in classical theorem has regularity following geometrical progression, we constructed one of the simplest models for heterogeneity. That is, assume that $\beta_j=\beta\rho^{j-1}$, where the unknown parameter ρ describes the index of heterogeneity of the target size. Then, the survival function in equation (2) can be specified as

$$S_k(D|\beta, \rho) = 1 - \prod_{j=1}^{k}(1 - e^{-\beta\rho^{j-1}D}). \quad (3)$$

From a graphical point of view, in the case that the number of targets k=10 for a given exposure dose (D), the heterogeneity index value of ρ>1 provides significant decreases in the survival curve as compared with that of ρ=1, as shown in Fig. 1. Continued increases in the value of ρ may give accelerated increases in the hazard rate.

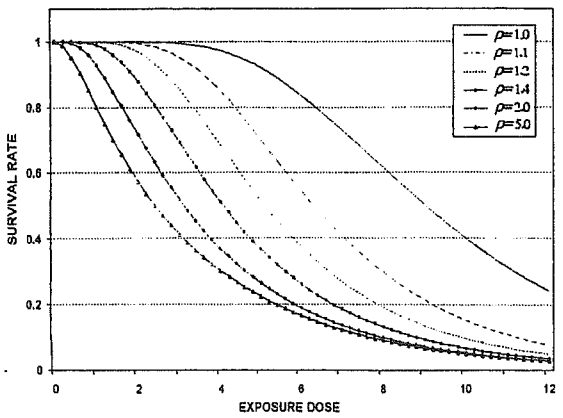

Fig. 1. Survival curves of the multi-target models at various values of ρ and given exposure dose (D), in a case where the number of targets k is equal to 10 and where the coefficient of exposure effects (β) is fixed. Significant decreases in the survival curve can be seen when the index value of ρ is greater than 1. A steady increase in the value of ρ results in an accelerated increase in the hazard rate.

2. Poisson Regression Model

Let Y be a response variable following Poisson distribution with mean $\mu_k(D, \boldsymbol{x}|\theta^*)=\mu_0 S_k(De^{\gamma^T\boldsymbol{x}}|\beta, \rho)$, a function of exposure dose (D) for given covariates vector $\boldsymbol{x}$ and unknown parameters vector $\theta^*=(k, \mu_0, \beta, \rho, \gamma^T)^T$, where μ_0 denotes the baseline mean parameter and $S_k(De^{\gamma^T\boldsymbol{x}}|\beta, \rho)$ expresses the survival function, which is specified as

$$S_k(De^{\gamma^T\boldsymbol{x}}|\beta, \rho) = 1 - \prod_{j=1}^{k}(1 - e^{-\beta\rho^{j-1}De^{\gamma^T\boldsymbol{x}}}), \quad (4)$$

where $\gamma^T\boldsymbol{x} = \gamma_1 x_1 + \gamma_2 x_2 + \cdots + \gamma_p x_p$ is a linear combination of p covariates. Then,

$$P(y|D, \boldsymbol{x}, \theta^*) = \frac{\{\mu_k(D, \boldsymbol{x}|\theta^*)\}^y}{y!} e^{-\mu_k(D,\boldsymbol{x}|\theta^*)}. \quad (5)$$

Given a set of n independent samples $(y_i, D_i, \boldsymbol{x}_i), i$=1,2, ... , n, where y_i is the observed response, D_i is the exposure dose and $\boldsymbol{x}_i=(x_{i1}, x_{i2}, \ldots, x_{ip})^T$ is the covariates vector for the ith individual, we denote the actually observed data set by $\boldsymbol{d}_{(obs)}=(\boldsymbol{y}, \boldsymbol{D}, \boldsymbol{x}^T)^T$. Then, the likelihood function for estimating the unknown parameters based on the observed data set can be specified by

$$L(\theta^*|\boldsymbol{d}_{(obs)}) = \prod_{i=1}^{n} P(y_i|D_i, \boldsymbol{x}_i, \theta^*). \quad (6)$$

3. Gamma-frailty Model for Heterogeneous Background

It is important to take account of heterogeneity between individuals in population-based survival studies[9]. A systematic way of describing heterogeneity is by entering an unobserved quantity called frailty, here denoted by the letter Z. This quantity describes common risk factors, measurable or non-measurable, and is not included in the model[9,10,22].

Till now, most studies have used a frailty having a gamma distribution, which is mathematically convenient. Gamma distributions have been used for many years to generate a Poisson mixture model. From a computational point of view, they fit

very well with survival models, because it is easy to derive the formulas for any number of events[9]. For finite mean frailty distributions, it is required that the mean of the frailty be unity in order for the parameters of the model to be identifiable[10]. Furthermore, regarding the heterogeneous population, Hougaard[8] has examined the consequences of the difference between gamma distribution and inverse Gaussian distribution as the distribution of frailties, and remarked that the inverse Gaussian makes the population homogeneous with time, whereas for the gamma the relative heterogeneity is constant. For these reasons, we adopt the gamma distribution as the distribution of frailties.

Assume that the mean of the survival rate at given exposure dose D is

$$\mu_k(D, \boldsymbol{x}|Z, \boldsymbol{\theta}^*) = Z\mu_k(D, \boldsymbol{x}|\boldsymbol{\theta}^*),$$

where Z denotes a random variable having gamma distribution with mean unity and variance σ (unknown). Then, the density function of Z can be described as

$$\varphi(z|\sigma) = \frac{\sigma^{-\sigma^{-1}}}{\Gamma(\sigma^{-1})} z^{\sigma^{-1}-1} e^{-\sigma^{-1}z}. \tag{7}$$

Let $\boldsymbol{d}=(y,D,\boldsymbol{x}^T,z)^T$ be the complete data set including the unobserved frailty term Z. The likelihood function can be formulated for a given complete data set $\boldsymbol{d}$ as

$$L(\boldsymbol{\theta}^*|\boldsymbol{d}) = \prod_{i=1}^{n} P(y_i|z_i, D_i, \boldsymbol{x}_i, \boldsymbol{\theta}^*), \tag{8}$$

where $P(y|z, D, \boldsymbol{x}, \boldsymbol{\theta}^*)$ denotes the probability density function of Poisson distribution with mean $\mu_k(D, \boldsymbol{x}|z, \boldsymbol{\theta}^*)$. Thus, the likelihood function based on the observed data set $\boldsymbol{d}_{(obs)}$ excluding the frailty term Z is obtained by integrating the likelihood function in equation (8) with respect to the density function of the frailty term of the ith individual, z_i. And, we have

$$\begin{aligned} L(\boldsymbol{\theta}|\boldsymbol{d}_{(obs)}) &= \int_0^\infty L(\boldsymbol{\theta}^*|\boldsymbol{d})\ \varphi(z_i|\sigma)\ dz_i \\ &= \prod_{i=1}^{n} \int_0^\infty P(y_i|z_i, D_i, \boldsymbol{x}_i, \boldsymbol{\theta}^*)\ \varphi(z_i|\sigma)\ dz_i \\ &= \prod_{i=1}^{n} f(y_i|D_i, \boldsymbol{x}_i, \boldsymbol{\theta}), \end{aligned} \tag{9}$$

where $f(y|D, \boldsymbol{x}, \boldsymbol{\theta})$ denotes the density function of negative binomial distribution with parameters vector $\boldsymbol{\theta} = (\boldsymbol{\theta}^{*T}, \sigma)^T$ expressed by

$$f(y|D, \boldsymbol{x}, \boldsymbol{\theta}) = \frac{\prod_{j=1}^{y}\{1+\sigma(j-1)\}}{y!} \left\{\frac{\mu(D, \boldsymbol{x}|\boldsymbol{\theta}^*)}{1+\sigma\mu(D, \boldsymbol{x}|\boldsymbol{\theta}^*)}\right\}^y \{1+\sigma\mu(D, \boldsymbol{x}|\boldsymbol{\theta}^*)\}^{-\sigma^{-1}} \tag{10}$$

PARAMETER ESTIMATION

The maximum likelihood estimation method based on the log-likelihood function on the observed data set $\boldsymbol{d}_{(obs)}$ is applied for estimating unknown parameters $\boldsymbol{\theta}$. The function can be written as

$$\ell(\boldsymbol{\theta}|\boldsymbol{d}_{(obs)}) = \log L(\boldsymbol{\theta}|\boldsymbol{d}_{(obs)}). \tag{11}$$

In many cases, an analytical method is not available for maximizing the function. Therefore, the maximization must be performed using a numerical method, often of an iterative character. The Newton-Raphson method, with its combination of simplicity and power, is the most widely used, although in general we know very little about its global convergence properties[11]. The method often becomes impractical in problems involving many parameters.

Ohtaki & Izumi[18], therefore, have proposed an algorithm called SPIDER for optimization without derivatives of the function. For the p-dimensional function, this alternative technique has iterative maximization procedures with cyclic fixing of groups of parameters, maximizing over the remaining parameters. (*The steps of the algorithm are presented in Appendix C*)

According to the general asymptotic theory, the maximum likelihood estimator has many useful properties, including consistency and sufficiency. The ability to achieve the Cramer-Rao minimum variance asymptotically is another remarkable property of the estimator. Under the regularity conditions, the vector of maximum likelihood estimators of $\boldsymbol{\theta}$ denoted by $\hat{\boldsymbol{\theta}}$ is best asymptotically normal (BAN) if $^\forall\boldsymbol{\theta} \in \Theta$, then $\hat{\boldsymbol{\theta}}$ is the approximation to the normal distribution with mean $\boldsymbol{\theta}$ and variance-covariance matrix $\frac{1}{n}I_1(\boldsymbol{\theta})^{-1}$ as n goes to infinity[14], or more explicitly we have

$$\sqrt{n}(\hat{\boldsymbol{\theta}} - \boldsymbol{\theta}) \sim N(0, I_1(\boldsymbol{\theta})^{-1}),$$

where $I_1(\boldsymbol{\theta})$ is the Fisher information matrix of sample size 1. Furthermore, the Fisher information matrix of sample size n, that is $I_n(\boldsymbol{\theta})=nI_1(\boldsymbol{\theta})$, is given by the symmetric matrix expressed as a negative form of expectation of the Hessian matrix whose ij-th element is specified by

$$I_n(\boldsymbol{\theta})_{i,j} = -E\left[\frac{\partial^2 \ell(\boldsymbol{\theta}|\boldsymbol{d}_{(obs)})}{\partial\theta_i\ \partial\theta_j}\right].$$

Moreover, inverting the form of the information matrix yields a matrix containing the variances of the parameters on its diagonal and the asymptotic covariance in the off-diagonal positions. The Hessian matrix elements of the models are described in detail in Appendix B.

APPLICATION TO REAL DATA ANALYSIS

1. Data Set

As an example of an application of multi-target models in the biomedical field, we will attempt to analyze experimental data on the density of the small intestinal crypt of mice after exposure to gamma rays. The aim of the experiment conducted by Ohara et al[16] was to verify the effect of giving a diet supplemented with miso (Japanese fermented soy bean paste) at various fermentation stages on crypt survival.

For this experiment, the mice were fed a commercial diet MF alone or a diet supplemented with miso for one week before the exposure. The miso had been fermented for a short-term (immediate fermentation), medium-term (4 months) or long-term (6 months). Groups of mice (each 5 mice) were whole-body exposed to 7, 8, 10 or 12 Gy of X-rays without anaesthetization. The number of surviving crypts was counted in 10 gut cross sections in each mouse.

2. Model for Growth and Disappearance of Intestinal Crypt

Ohara et al[16] remarked that in the absence of surviving crypt stem cells, the crypts disappear. In both the large and small intestine, mutagen administration leads to the occurrence of isolated crypts that are completely populated by a mutated phenotype. Therefore, it has been proposed that crypts are maintained by a single stem cell.

On the other hand, the results of studies on the small intestine by Williams et al[24] lead them to question the previous assumption. They proposed an alternative hypothesis in regard to the number of stem cells required to maintain the crypts, and gave an explanation based on multiple crypt stem cells with random cell loss after stem cell division.

Consider that a crypt contains multiple stem cells, and let the (unknown) parameter be m. Suppose that all of the stem cells will disappear after k independent hits cause the crypt to cease growing. Then, for given exposure dose D and covariates vector $\boldsymbol{x}=(x_1,x_2,x_3)^T$, we can apply the survival function in equation (4) with a slight modification for the survivor crypt data:

$$S_{k,m}(De^{\gamma^T x}|\beta,\rho)=1-\left\{\prod_{j=1}^{k}\left(1-e^{-\beta\rho^{j-1}De^{\gamma^T x}}\right)\right\}^m, \quad (12)$$

where the covariates vector $\boldsymbol{x}$ is constructed by setting a dummy variable to account for the duration of fermentation:

$$x_1=\begin{cases}1, \text{ if "Early" (short-term fermentation),}\\ 0, \text{ otherwise}\end{cases}$$

$$x_2=\begin{cases}1, \text{ if "Medium" (medium-term fermentation),}\\ 0, \text{ otherwise}\end{cases}$$

$$x_3=\begin{cases}1, \text{ if "Long" (long-term fermentation),}\\ 0, \text{ otherwise}\end{cases}$$

3. Results

The results show that there are substantial frailties for all miso fermentation-stages. The Akaike Information Criterion (AIC) values as a fit-

Table 1. Estimated Parameter Values in the Non-Frailty Poisson Regression Model

A. Homogeneous multi-target model

Number of targets	$\hat{\beta}$	$\hat{\rho}$	$\widehat{RR}_e$	$\widehat{RR}_m$	$\widehat{RR}_l$	*AIC*
12	0.3163 (0.3092, 0.3233)	1.0	0.913	0.921	0.871	1253.12

B. Heterogeneous multi-target model with single stem cell assumption

Number of targets	$\hat{\beta}$	$\hat{\rho}$	$\widehat{RR}_e$	$\widehat{RR}_m$	$\widehat{RR}_l$	*AIC*
10	0.2609 (0.2602, 0.2617)	1.035	0.910	0.919	0.869	1261.14
20	0.2356 (0.2351, 0.2361)	1.069	0.912	0.921	0.871	1236.30
30	0.2357 (0.2354, 0.2361)	1.069	0.912	0.921	0.871	1235.28
40	0.2358 (0.2355, 0.2361)	1.069	0.912	0.921	0.871	1235.28

C. Heterogeneous multi-target model with multiple stem cell assumption

Number of stem cells	Number of targets	$\hat{\beta}$	$\hat{\rho}$	$\widehat{RR}_e$	$\widehat{RR}_m$	$\widehat{RR}_l$	*AIC*
2	10	0.2430 (0.2425, 0.2434)	1.144	0.912	0.921	0.871	1236.38
	15	0.2432 (0.2428, 0.2435)	1.143	0.912	0.921	0.871	1235.40
	20	0.2432 (0.2429, 0.2434)	1.144	0.912	0.921	0.871	1235.40
3	10	0.2505 (0.2501, 0.2508)	1.225	0.912	0.921	0.871	1235.61
	12	0.2504 (0.2501, 0.2507)	1.225	0.912	0.921	0.871	1235.60
4	8	0.2576 (0.2573, 0.2580)	1.314	0.912	0.921	0.871	1235.90
	10	0.2576 (0.2573, 0.2579)	1.314	0.912	0.921	0.871	1235.90

Note: Values in parentheses are the 95% confidence intervals